

Chattering-free terminal sliding mode control based on adaptive exponential reaching barrier function for a chaotic permanent magnet synchronous generator in offshore wind turbine system

Aissa Benabdeseelam, Manal Messadi, Karim Kemih, Hamid Hamiche

Citation: Chin. Phys. B, 2025, 34 (**9**): 090501. DOI: 10.1088/1674-1056/add248
http://cpb.iphy.ac.cn; http://iopscience.iop.org/cpb

What follows is a list of articles you may be interested in

An enhanced fingerprint template protection scheme based on four-dimensional superchaotic system and dynamic DNA coding

Baiqiang Hu(胡百强), Jiahui Liu(刘嘉辉), and Zhe Liu(刘喆)
Chin. Phys. B, 2025, 34 (**7**): 070505. DOI: 10.1088/1674-1056/adca9f

Model-free prediction of chaotic dynamics with parameter-aware reservoir computing

Jianmin Guo(郭建敏), Yao Du(杜瑶), Haibo Luo(罗海波), Xuan Wang(王晅), Yizhen Yu(于一真), and Xingang Wang(王新刚)
Chin. Phys. B, 2025, 34 (**4**): 040505. DOI: 10.1088/1674-1056/adb733

A novel approach to visual image encryption: 2D hyperchaos, variable Josephus, and 3D diffusion

Yan Hong(洪炎), Xinyan Duan(段心妍), Jingming Su(苏静明), Zhaopan Wang(王昭盼), and Shihui Fang(方士辉)
Chin. Phys. B, 2025, 34 (**4**): 040504. DOI: 10.1088/1674-1056/adacc7

A color image encryption scheme based on a 2D coupled chaotic system and diagonal scrambling algorithm

Jingming Su(苏静明), Shihui Fang(方士辉), Yan Hong(洪炎), and Yan Wen(温言)
Chin. Phys. B, 2024, 33 (**7**): 070502. DOI: 10.1088/1674-1056/ad3efa

Two-dimensional-lag complex logistic map with complex parameters and its encryption application

Fangfang Zhang(张芳芳), Jinbo Wu(武金波), Lei Kou(寇磊), Fengying Ma(马凤英), Liming Wu(吴黎明), and Xue Zhang(张雪)
Chin. Phys. B, 2024, 33 (**5**): 050505. DOI: 10.1088/1674-1056/ad2a69

Chattering-free terminal sliding mode control based on adaptive exponential reaching barrier function for a chaotic permanent magnet synchronous generator in offshore wind turbine system

Aissa Benabdeseelam[1], Manal Messadi[1], Karim Kemih[1,†], Hamid Hamiche[2]

[1] *L2EI Laboratory, Jijel University, BP* 98 *Ouled Aissa, Jijel* 18000, *Algeria*

[2] *Laboratoire de Conception et Conduite des Systèmes de Production (L2CSP), Mouloud Mammeri University, Tizi-Ouzou, Algeria*

(Received 12 March 2025; revised manuscript received 27 April 2025; accepted manuscript online 30 April 2025)

This paper introduces a novel chattering-free terminal sliding mode control (SMC) strategy to address chaotic behavior in permanent magnet synchronous generators (PMSG) for offshore wind turbine systems. By integrating an adaptive exponential reaching law with a continuous barrier function, the proposed approach eliminates chattering and ensures robust performance under model uncertainties. The methodology combines adaptive SMC with dynamic switching to estimate and compensates for unknown uncertainties, providing smooth and stable control. Finally, the performance and effectiveness of the proposed approach are compared with those of a previous study.

Keywords: permanent magnet synchronous generator, chaotic system, terminal sliding mode control, exponential reaching, adaptive barrier function, chattering-free, unknown uncertainty

PACS: 05.45.Gg, 02.30.Yy, 05.45.–a, 05.45.Pq

DOI: 10.1088/1674-1056/add248 **CSTR:** 32038.14.CPB.add248

1. Introduction

In recent years, wind energy production has seen rapid growth, fueled by escalating concerns over the environmental impact of fossil fuel depletion and the related emissions that contribute to climate change. Despite significant advancements in wind energy technology over the past few decades, there remains a pressing need for further innovations to develop wind turbines that are not only reliable but also cost-effective for widespread use.[1,2] A critical component of this technology is the wind turbine's generator, which plays a crucial role in converting the kinetic energy harnessed by the rotor from moving air into usable electrical energy.[3,4] As the demand for sustainable energy sources continues to rise, enhancing the efficiency and affordability of wind turbines will be essential for expanding the renewable energy landscape.

Offshore wind turbines, also known as marine wind turbines, use different types of generators to convert the mechanical energy generated by the movement of the blades due to the wind into electrical energy. Among these generators are the doubly fed induction generator (DFIG), the doubly salient electromagnetic generator (DSEG), and the permanent magnet synchronous generator (PMSG), each with specific characteristics suited to different applications. The choice of generator used in an offshore wind turbine depends on several factors, including the specific application, power requirements, and the operating conditions of the wind area. For example, induction generators (such as the DFIG) are commonly used in large-scale wind systems due to their ability to maintain a constant frequency while allowing flexible power regulation.[4] However, these systems may require more complex control equipment. In contrast, permanent magnet generators, like the PMSG, are becoming increasingly popular due to their numerous advantages. The PMSG stands out for its features that make it particularly well suited for modern wind turbines. Some of its key benefits include relatively low manufacturing costs compared to other types of generators, making it economically viable. Additionally, it allows for high operating speeds while maintaining great stability, which is essential for optimizing energy production in variable wind conditions. Its compact size also makes it an advantageous choice, especially in installations with limited space or for small to medium-sized turbines. Another major advantage of the PMSG is its impressive efficiency, thanks to reduced energy losses, which improves overall system performance. The PMSG also offers an excellent torque-to-inertia ratio, allowing for better speed regulation and a faster response to changes in wind speed. Its high-power density enables the maximization of energy production while minimizing the size of the generator. Due to these numerous advantages, the PMSG has become a common configuration in modern wind systems. It is also an increasingly attractive option for application generators in fields beyond wind energy, including industrial applications and elec-

†Corresponding author. E-mail: k.kemih@gmail.com

© 2025 Chinese Physical Society and IOP Publishing Ltd. All rights, including for text and data mining, AI training, and similar technologies, are reserved.

tric vehicles. The potential for managing the PMSG, particularly in the context of hybrid power systems or advanced control systems, has generated growing interest among researchers in recent years. Many studies focus on optimizing the performance of the PMSG, improving system reliability, and reducing energy production costs, which is helping accelerate its adoption in various industrial and commercial applications.[6]

The PMSG is a quintessential high nonlinearity, multivariable coupled system, exhibiting significant sensitivity to load disturbances, frictional forces, and parameter variations when the motor shaft is directly connected to an external load. According to certain research, when system parameters fall within a particular range, the PMSG exhibits chaotic behavior.[7,8] PMSG's chaotic behavior, which mostly manifests as low-frequency oscillations of the motor's rotational speed and sporadic torque ripples, can seriously impair the motor's stabilization and potentially cause the drive system to collapse. Achieving optimal dynamic performance of the PMSG in real-world applications presents significant challenges due to all these factors.[1] The task of mitigating chaos in PMSG has attracted considerable attention in the field of nonlinear control for electric motors. To date, a variety of control strategies have been explored and applied to successfully suppress and manage chaos in PMSG systems.[8–13]

Chaos theory is a field of mathematics that explores systems that appear random or unpredictable, despite being governed by deterministic laws.[14] These systems are highly sensitive to initial conditions, meaning that small changes can lead to vastly different outcomes, a phenomenon often referred to as the "butterfly effect".[15] In engineering, chaos theory has significant applications across various disciplines. It helps engineers understand and control complex, nonlinear systems in fields such as control systems, mechanical vibrations, fluid dynamics, electrical circuits, and structural design. By applying chaos theory, we can predict and mitigate instability, optimize performance, and enhance the reliability of systems, even in the face of apparent randomness. From stabilizing power grids to improving aerodynamic designs and enhancing signal processing, chaos theory has become an essential tool for addressing real-world challenges in modern engineering.[16]

Numerous researchers have given the chaos control problem a great deal of attention, since Ott *et al*. first considered it in 1990.[17] Nowadays, several control techniques have been devised to regulate chaotic systems, including the sliding mode control,[18–21] the adaptive control,[22–25] the backstepping,[26,27] the passivity feedback control,[28–30] the constrained generalized predictive control,[31] the predictive control,[32–34] the impulsive method,[35–37] and the barrier function-based sliding mode control methods,[38–40] are a few examples.

Sliding mode control (SMC) is recognized as a powerful and robust strategy for managing chaos within chaotic systems.[41,42] Nevertheless, numerous traditional SMC methods face the challenge of chattering, a phenomenon that arises from the discontinuities present in the control input due to the signum function. A new control technique has been created to tackle the chattering issue found in sliding mode controllers, proving to be a superior solution over conventional methods like saturation functions and higher-order derivatives of sliding manifolds. This cutting-edge method, termed "sliding mode control based on the adaptive continuous barrier function," utilizes an adaptive continuous barrier function to formulate a seamless and continuous control strategy for the switching surface, effectively eliminating the chattering problem in sliding mode control. Its simplicity, robustness, and real-world effectiveness distinguish it from earlier approaches. Plestan *et al*. were the first to suggest the barrier function-based SMC.[43] This strategy was later used in a variety of research studies.[44–46] The suggested barrier approach ensures that the outputs converge to the origin without overstating the control gain, even with uncertain boundaries.

The authors in Ref. [47] took the dynamic sliding mode surface approach established in Ref. [22] and enhanced it significantly by integrating an adaptive continuous barrier function into the switch function. This innovative addition aims to effectively mitigate the issue of chatter. The advancements made in this work showcase a thoughtful progression in the methods used for improving control system performance.

In this paper, an adaptive exponential reaching barrier function is proposed and integrated into the switching function previously introduced in Ref. [47], with the objective of mitigating chattering effects and improving the overall robustness of the control strategy. We aim to implement this approach in the chaotic system described in Ref. [34], which serves as the primary objective of our research. By applying this technique, we expect to improve the stability and performance of the chaotic system under various operating conditions.

The paper is organized as follows: Section 2 introduces brief preliminaries on the modeling of the wind turbine. Section 3 is devoted to giving the system description, while Section 4 is dedicated to the proposed control and its stability synthesis. Section 5 is devoted to the application of the suggested control on the chaotic PMSG. Finally, our main conclusion and future works are summed up in Section 6.

2. Modeling the wind turbine

Figure 1 illustrates the configuration of a PMSG wind turbine.

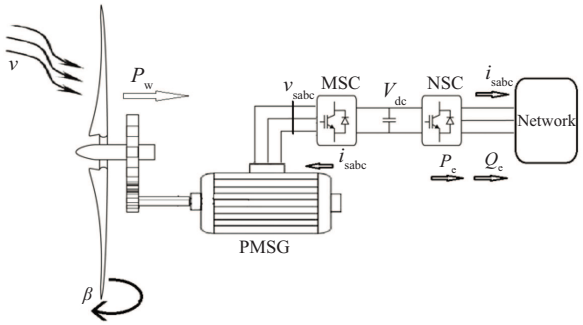


Fig. 1. Schematic design of a PMSG-based wind turbine. v: wind; P_w: wind energy; MSC: machine side converter; NSC: network side converter; β: pitch angle; v_{sabc}: stator three-phase voltage; i_{sabc}: stator three-phase current; v_{dc}: dc-link voltage; P_e: the active output power; Q_e: the reactive output power; i_{labs}: load current.

The variable-speed wind turbine is a sophisticated electromechanical system comprising various mechanical components, including the direct-drive PMSG, among others. A detailed overview of these components will be provided below.[34]

2.1. Wind turbine aerodynamic model

The power recovered by the wind turbine rotor is given by the following equation:

$$P_w = \frac{1}{2}\rho\pi R^2 V_w^3 C_p, \tag{1}$$

where ρ is the air density (in units kg/m^3), R is the blade length (in unit m), and V_w is the wind speed (in units m/s). C_p is the power coefficient; it depends on β and λ. It is given by[4]

$$c_p(\lambda,\beta) = c_1\left[c_2\left(\frac{1}{\lambda+0.08\beta}-\frac{0.035}{\beta^3+a}\right)-c_3\beta-c_4\right]\exp-\left(\frac{1}{\lambda+0.08\beta}-\frac{0.035}{\beta^3+1}\right)+c_6\lambda, \tag{2}$$

with $c_1 = 0.5109$, $c_2 = 116$, $c_3 = 0.4$, $c_4 = 5$, $c_5 = 21$, $c_6 = 0.0068$. λ represents the speed ratio. It is given by[34]

$$\lambda = \frac{wR}{V_w}, \tag{3}$$

where w is the rotor's angular speed. When $\lambda = \lambda_{opt}$ (the optimum value of λ, C_p reaches its peak value C_{pmax}, as illustrated in Fig. 2.

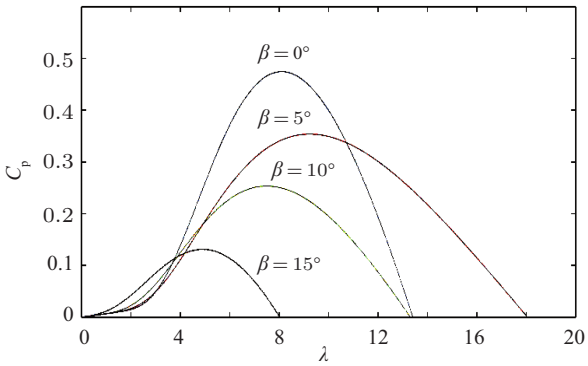


Fig. 2. Curves of the wind turbines power coefficient C_p.[34]

Based on Eqs. (2) and (3), the optimal power captured, denoted as P_{opt}, can be expressed as

$$P_{opt} = \frac{1}{2}\rho\pi R^2 C_{pmax}\left[\left(\frac{R}{\lambda_{opt}}\right)w\right]^3, \tag{4}$$

2.2. The PMSG model

The DC motor exhibits outstanding control capabilities. As a result, our goal is to transform the PMSG into a DC motor by transitioning from a three-phase stationary reference frame to a two-phase synchronous reference frame. The process for this transformation is outlined below.

(i) Transform the 3-phase *abc* stationary reference frame into a 2-phase α and ψ stationary reference frame. For instance, consider the conversion of three-phase voltages,[34]

$$\begin{bmatrix} u_\alpha \\ u_\psi \end{bmatrix} = \begin{bmatrix} 1 & -1/2 & -1/2 \\ 0 & \sqrt{3}/2 & -\sqrt{3}/2 \end{bmatrix}\begin{bmatrix} u_a \\ u_b \\ u_c \end{bmatrix}. \tag{5}$$

(ii) The two-phase α and ψ systems are stationary within a two-phase synchronous rotational reference frame. For instance, consider the two-phase voltages,

$$\begin{bmatrix} u_d \\ u_q \end{bmatrix} = \begin{bmatrix} \cos\theta & \sin\theta \\ -\sin\theta & \cos\theta \end{bmatrix}\begin{bmatrix} u_\alpha \\ u_\psi \end{bmatrix}, \tag{6}$$

It is important to note that the conversion process is analogous to other variables as well. By applying a sequence of conversions akin to those in Eqs. (5) and (6), we ultimately derive the final mathematical models

$$\begin{aligned} \frac{dw}{dt'} &= \frac{p}{J}\left(\varnothing_f i_q + \left(L_d - L_q\right) i_d i_q\right) - \frac{f}{J}w - \frac{T_l}{J}, \\ \frac{di_q}{dt'} &= -\frac{R_s}{L_q}i_q + \frac{L_d}{L_q}pwi_d - \frac{p\varnothing_f}{L_q}w + \frac{u_q}{L_d}, \end{aligned} \tag{7}$$

where u_d and u_q are the control voltages for the direct and quadrature axis stator, i_q and i_d are the stator currents for both the quadrature and direct axes, L_d and L_q refer to the inductance values in the direct and quadrature axis of the stator, p is the poles pairs number, R_s is the stator resistance, $\varnothing_f$ is the magnetic flux of the rotor linked to the stator, T_l is the load torque, J represents the moment of inertia of the rotor, f is the coefficient of viscous friction, t represents time.[34]

Through the use of an affine and a temporal scaling transformation, equation (7) can be reformulated as[11]

$$\begin{cases} \dfrac{\mathrm{d}\tilde{w}}{\mathrm{d}t} = \varphi\left(\tilde{i}_{\mathrm{q}} - \tilde{w}\right) + \varepsilon\tilde{i}_{\mathrm{d}}\tilde{i}_{\mathrm{q}} - \tilde{T}, \\ \dfrac{\mathrm{d}\tilde{i}_{\mathrm{q}}}{\mathrm{d}t} = -\tilde{i}_{\mathrm{q}} - \tilde{w}\tilde{i}_{\mathrm{d}} + \gamma\tilde{w} + \tilde{u}_{\mathrm{q}}, \\ \dfrac{\mathrm{d}\tilde{i}_{\mathrm{d}}}{\mathrm{d}t} = -\tilde{i}_{\mathrm{d}} + \tilde{w}\tilde{i}_{\mathrm{q}} + \tilde{u}_{\mathrm{d}}, \end{cases} \tag{8}$$

where

$$\varepsilon = \frac{pbL_{\mathrm{q}}^2k^2\left(L_{\mathrm{q}} - L_{\mathrm{d}}\right)}{JR_{\mathrm{s}}^2}, \quad \gamma = -\frac{\varnothing_{\mathrm{f}}}{kL_{\mathrm{q}}}, \quad \varphi = \frac{fL_{\mathrm{q}}}{R_{\mathrm{s}}J},$$
$$b = \frac{L_{\mathrm{q}}}{L_{\mathrm{d}}}, \quad k = \frac{fR}{L_{\mathrm{q}}p\varnothing_{\mathrm{f}}}, \quad \tilde{i}_{\mathrm{d}} = \frac{L_{\mathrm{d}}p\varnothing_{\mathrm{f}}}{fR_{\mathrm{s}}}i_{\mathrm{d}},$$
$$\tilde{i}_{\mathrm{q}} = \frac{L_{\mathrm{q}}p\varnothing_{\mathrm{f}}}{fR_{\mathrm{s}}}i_{\mathrm{q}}, \quad \tilde{w} = \frac{L_{\mathrm{q}}}{R_{\mathrm{s}}}w,$$
$$\tilde{u}_{\mathrm{d}} = \frac{1}{R_{\mathrm{s}}k}u_{\mathrm{d}}, \quad \tilde{u}_{\mathrm{q}} = \frac{1}{R_{\mathrm{s}}k}u_{\mathrm{q}}, \quad \tilde{T} = \frac{L_{\mathrm{q}}^2}{JR_{\mathrm{s}}^2}T_1,$$

and the time will be redefined to $t = R_{\mathrm{s}}t'/L_{\mathrm{q}}$.

we put $x_1 = \tilde{w}$, $x_2 = \tilde{i}_{\mathrm{q}}$, $x_3 = \tilde{i}_{\mathrm{d}}$.

We may convert the previously PMSG model (8) into the following normalized PMSG model

$$\begin{cases} \dot{x}_1 = \varphi\left(x_2 - x_1\right) + \tilde{T} + \varepsilon x_3x_2, \\ \dot{x}_2 = -x_2 - x_1x_3 + \gamma x_1 + \tilde{u}_{\mathrm{q}}, \\ \dot{x}_3 = -x_3 + x_1x_2 + \tilde{u}_{\mathrm{d}}, \end{cases} \tag{9}$$

where the variable x represents a state vector expressed by $x = [x_1, x_2, x_3]^{\mathrm{T}}$.

According to the study, the PMSG exhibits chaotic behavior when the external inputs are initialized to zero, specifically $\tilde{T} = \tilde{u}_{\mathrm{q}} = \tilde{u}_{\mathrm{d}} = 0$, and the operational parameters φ and γ fall within a specific range. Figure 3 shows the chaotic attractor of the PMSG system with $\varphi = 5.45$ and $\gamma = 20$ with the initial state values $x(0) = [0.1, 0.3, 0.2]^{\mathrm{T}}$.

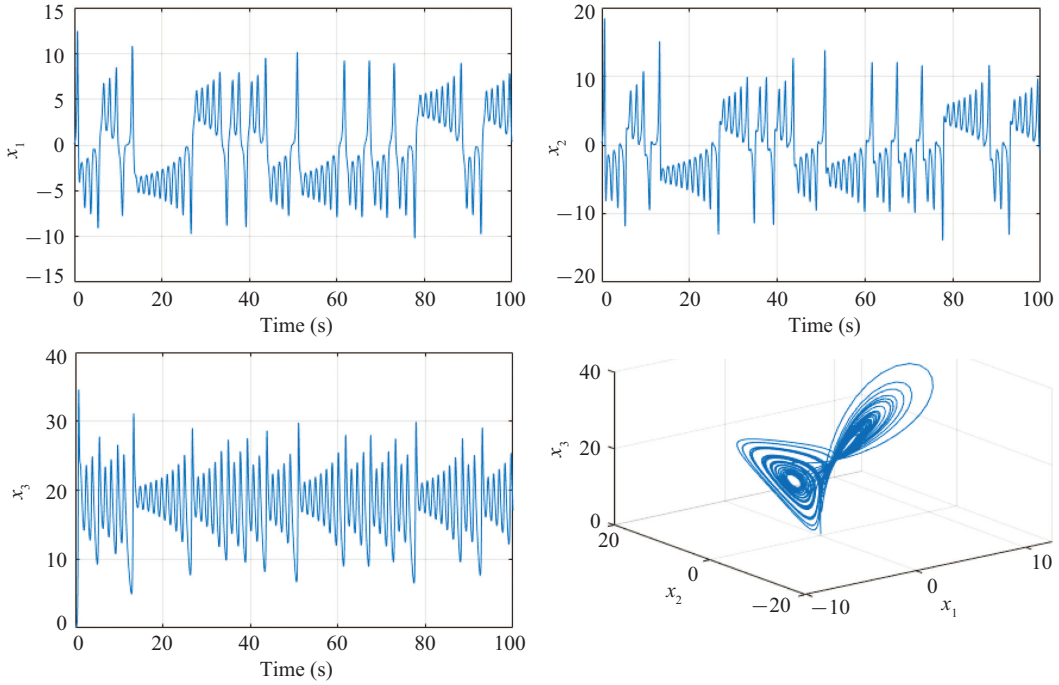


Fig. 3. State variable of the chaotic PMSG in the absence of control and the characteristic chaotic attractor.

3. System description

Nonlinear dynamics often describe chaotic systems through the following dynamic equations:

$$\dot{x} = f(t,x) + d(t,x) + u(t), \tag{10}$$

where $\dot{x} = [x_1, x_2, \ldots, x_n]^{\mathrm{T}} \in R^n$ denotes the system state vector, $f(t,x) : R^+ \times R^n \to R^n$ represents a continuous nonlinear vector field, $d(t,x) : R^+ \times R^n \to R^n$ signifies the term unknown uncertainty, encompassing model uncertainties, unmodeled dynamics within the system, unforeseen external disturbances, and $u(t) \in R^n$ is the control input. The chaotic system's equation (10) assumes that the quantity of state variables $x$equals the control inputs u.

The objective of this paper is to develop a robust and adaptive TSMC law for uncertain chaotic PMSG under unknown external disturbances, ensuring that the stability of the overall system's state:

$$\|x(t)\| = 0. \tag{11}$$

Remark 1 It is evident that if $f(t,x) = Bx + F(t,x)$ and $d(t,x) = d(t)$, then dynamic equation (10) reduces to the fol-

lowing dynamic equation, defined in Ref. [18]:

$$\dot{x} = Bx + F(t,x) + d(t) + u(t). \tag{12}$$

In contrast to the term of uncertainty $d(t)$ defined in Ref. [18], where x is independent of time t, the problem is explained and formulated in this article under the assumption that the vector of the state variable x depends on the unknown time t in the uncertainty term $d(t,x)$.

Lemma 1[41] Let $x \in M \subset R^n$ and $\dot{x} = g(x)\, g : R^n \to R^n$ is continuous in an open neighborhood M of the origin and locally Lipshitz on $M\{0\}$ and $g(0) = 0$, suppose there is a continuous Lyapunov function $V : M \to R$ such that the subsequent conditions are met.

(i) V is positive-specific;

(ii) $\dot{V}$ is negative-specific on M;

(iii) There exist positive real values m and $a \in (0;1)$, with a neighborhood $M \subset M$ of the origin so that

$$\dot{V} + mV^a \leq 0; \text{ on the } M\{0\}. \tag{13}$$

Therefore, the origin serves as a stable equilibrium point for $\dot{x} = g(x)$, indicating that the trajectory of the system's states converges to the origin within a finite time frame.

4. Proposed control and its stability synthesis

To generate continuous, smooth, and differentiable control signals while weakening the chattering phenomena, the switching component of the discontinuous sliding surface is diverted into the control input's first derivative. As a consequence, the following sliding surface that provides a seamless adaptive law are specified

$$\sigma_i(t) = \dot{s}_i(t) + \lambda_i s_i(t), \tag{14}$$

where $\lambda_i\ (i = 1,2,\ldots,n)$ are positive constants, and sliding surfaces s_i is specified as follows:

$$s_i(t) = k_i \int_0^t x_i(\tau)\mathrm{d}\tau + x_i(t), \tag{15}$$

where k_i are positive constants, $x_i(t)$ denotes the system's state variables where $i = 1,2,\ldots,n$. A significant advantage of Eq. (15) is that it transforms sliding mode control (SMC) into global sliding mode control (GSMC) by using an integral and nonlinear switching function. This nonlinear sliding surface complies with the essential conditions of GSMC, namely $s(0) = 0$, $s(\infty) = 0$. Consequently, one of the main benefits of adopting these integral sliding manifolds is that the suggested scheme achieves GSMC status, effectively eliminating the reaching phase. By positioning the sliding surface from the outset, the controller exhibits robust performance, effectively countering uncertainties right from the beginning.

4.1. Optimizing the suggested controller using an adaptive exponential reaching barrier function

This work introduces an innovative control method, where we propose the implementation of a novel adaptive exponential reaching control law, which is thoughtfully constructed on the foundational principles of the adaptive continuous barrier function. This approach aims to enhance system performance by dynamically adjusting to changes in the environment and the system's state. By incorporating this advanced control law, we anticipate improved stability and responsiveness in various applications. Ultimately, our method seeks to facilitate more robust control mechanisms in complex scenarios.

The schematic diagram of the suggested control configuration is displayed in Fig. 4.

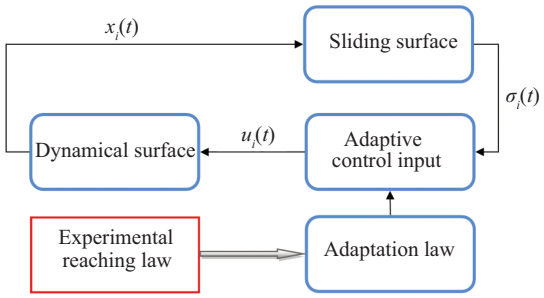


Fig. 4. Diagram of the control method using exponential reaching law.

Before proceeding further, we assume the following.

Assumption 1 In this context, we operate under the assumption that there exist unknown positive constants c_i, $i = 1,2,\ldots,n$, such that

$$\left|\sum_{j=1}^{n} \frac{\partial d_i(t,x)}{\partial x_j}\dot{x}_j + \frac{\partial d_i(t,x)}{\partial t}\right| + (\lambda_i + k_i)\left|d_i(t,x)\right| \leq c_i, \tag{16}$$

where $d_i(t,x)$ are the unknown uncertainty terms in Eq. (10) and $i = 1,2,\ldots,n$.

Remark 2 It is important to note that, in contrast to Ref. [18], we permit the upperbound parameter c_i to remain unknown.

Theorem 1[22] Based on assumption 1, if the adaptive TSMC is

$$\dot{u}_i = -(\lambda_i + k_i)(u_i + f_i(t,x)) - \sum_{j=1}^{n} \frac{\partial f_i(t,x)}{\partial x_j}\dot{x}_j - \frac{\partial f_i(t,x)}{\partial t} - \lambda_i k_i x_i - \varepsilon_i \hat{c}_i sign(\sigma_i), \tag{17}$$

where $\varepsilon_i > 1$, and $i = 1, 2, \ldots, n$ are a set of constant parameters associated with the controller design, $\hat{c}_i$ is an estimate of c_i the unknown upper bound and is given by

$$\dot{\hat{c}}_i = \varepsilon_i |\sigma_i| . \tag{18}$$

Lemma 2[40] The suggested control approach may be enhanced by utilizing the adaptive barrier function-based TSMC to accurately predict the system's unknown uncertainties, resulting in increased stability within the closed-loop system. To achieve this, the adaptation gain parameter $\hat{c}_i$ in Eq. (17) can be expressed as follows:[47]

$$\hat{c}_i(t) = \begin{cases} \hat{c}_{i_{\rm a}}(t), & \text{if } 0 < t < \bar{t}, \\ \hat{c}_{i_{\rm psd}}(t), & \text{if } t > \bar{t}, \end{cases} \tag{19}$$

where $\bar{t}$ denotes the time that the error converges to the neighborhood τ of the sliding surface dynamics $\sigma_i(t)$.

The proposed control method in Ref. [47] respectively includes an adaptation law and a positive-semi-definite continuous barrier function given as follows:

$$\dot{\hat{c}}_{i_{\rm a}} = \varepsilon_i |\sigma_i(t)| , \tag{20}$$

$$\dot{\hat{c}}_{i_{\rm psd}}(t) = \frac{|\sigma_i(t)|}{\tau_i - |\sigma_i(t)|} , \tag{21}$$

where $\tau > 0$.

Otherwise, in our proposed method, we draw inspiration from Ref. [48] and implement an adaptation rule. This approach allows us to create an optimized continuous barrier function, utilizing the exponential reaching law, as described by the following expression:

$$\dot{\hat{c}}_{i_{\rm opt}}(t) = \frac{K|\sigma_i(t)|}{\sigma_0 + (1-\sigma_0)\,{\rm e}^{-\alpha|\sigma_i(t)|^p}} , \tag{22}$$

where K, α are positive scalar parameters, p is the number of machine pole pairs and $0 < \sigma_0 < 1$.

For the case of $0 < t \le \bar{t}$, the proposed scheme utilizes the control law given in Eq. (17), while in scenarios involving $t > \bar{t}$, the control input is formulated using an adaptive law grounded in the barrier function:

$$\begin{aligned} \dot{u}_i = &-(\lambda_i + k_i)(u_i + f_i(t,x)) - \sum_{j=1}^{n} \frac{\partial f_i(t,x)}{\partial x_j}\dot{x}_j \\ &- \frac{\partial f_i(t,x)}{\partial t} - \lambda_i k_i x_i - \varepsilon_i \hat{c}_{i_{\rm opt}} \operatorname{sign}(\sigma_i) . \end{aligned} \tag{23}$$

Subsequently, as the trajectories of the system state approach the convergence zone of the sliding surface dynamics $\sigma_i(t)$, they ultimately converge to zero. Consequently, the closed-loop system achieves stability within a finite amount of time.

Remark 3 Based on Lemma 2, the suggested controller uses an adaptive exponential reaching barrier function in the SMC; this design ensures finite-time convergence and effectively stabilizes the closed-loop control system in a limited timeframe.[47]

Proof To establish the stability of the controller using control law (23), we can utilize the following Lyapunov candidate function:

$$V_i(t) = \frac{1}{2}\left(\sigma_i(t)^2 + \left(\hat{c}_{i_{\rm opt}}(t) - \hat{c}_{i_{\rm opt}}(0)\right)^2\right). \tag{24}$$

By applying the time derivative of Eq. (24), we obtain

$$\dot{V}_i(t) = \sigma_i(t)\dot{\sigma}_i(t) + (\hat{c}_{i_{\rm opt}}(t) - \hat{c}_{i_{\rm opt}}(0))\dot{\hat{c}}_{i_{\rm opt}}(t) , \tag{25}$$

where substituting $\dot{\sigma}_i(t)$ and $\hat{c}_{i_{\rm opt}}(0) = 0$ in the above equation, we will have

$$\begin{aligned} \dot{V}_i(t) = \sigma_i(t)\Bigg(&\sum_{j=1}^{n}\frac{\partial f_i(t,x)}{\partial x_j}\dot{x}_j + \frac{\partial f_i(t,x)}{\partial t} + \sum_{j=1}^{n}\frac{\partial d_i(t,x)}{\partial x_j}\dot{x}_j + \frac{\partial d_i(t,x)}{\partial t} + \dot{u}_i + (\lambda_i + k_i)(f_i(t,x) + d_i(t,x) + u_i) + \lambda_i k_i x_i\Bigg) \\ &+ \hat{c}_{i_{\rm opt}}(t)\dot{\hat{c}}_{i_{\rm opt}}(t) . \end{aligned} \tag{26}$$

Replacing the control rule $\dot{u}_i$ of Eq. (23) in Eq. (26) and employing Eq. (26), one can have

$$\begin{aligned} \dot{V}_i(t) &= \sigma_i(t)\left(-\varepsilon_i\hat{c}_{i_{\rm opt}}(t)\,sign(\sigma_i(t)) + d(t,x)\right) + \hat{c}_{i_{\rm opt}}(t)\dot{\hat{c}}_{i_{\rm opt}}(t) \\ &\le |\sigma_i(t)| \times \left\{|d(t,x)| - \varepsilon_i\hat{c}_{i_{\rm opt}}(t)\right\} + \hat{c}_{i_{\rm opt}}(t)\dot{\hat{c}}_{i_{\rm opt}}(t) \le |\sigma_i(t)| \times \left\{|d(t,x)| - \varepsilon_i\hat{c}_{i_{\rm opt}}(t)\right\} + \hat{c}_{i_{\rm opt}}(t) \\ &\quad \times \frac{K\left[\left(\sigma_0 + (1-\sigma_0)\,{\rm e}^{-\alpha|\sigma_i(t)|^p}\right) + |\sigma_i(t)|(1-\sigma_0)\,{\rm e}^{-\alpha|\sigma_i(t)|^p}\alpha p|\sigma_i(t)|^{p-1}\right]}{\left(\sigma_0 + (1-\sigma_0)\,{\rm e}^{-\alpha|\sigma_i(t)|^p}\right)^2} \\ &\quad \times \left[d(t,x) - \varepsilon_i\hat{c}_{i_{\rm opt}}(t)\operatorname{sign}(\sigma_i(t))\right]\operatorname{sign}(\sigma_i(t)) . \end{aligned} \tag{27}$$

Equation (27) gives the following inequality:

$$\begin{aligned} \dot{V}_i(t) \le &-\left\{\varepsilon_i\hat{c}_{i_{\rm opt}}(t) - |d(t,x)|\right\}|\sigma_i(t)| - \hat{c}_{i_{\rm opt}}(t) \\ &\times \frac{K\left[\left(\sigma_0 + (1-\sigma_0)\,{\rm e}^{-\alpha|\sigma_i(t)|^p}\right) + |\sigma_i(t)|(1-\sigma_0)\,{\rm e}^{-\alpha|\sigma_i(t)|^p}\alpha p|\sigma_i(t)|^{p-1}\right]}{\left(\sigma_0 + (1-\sigma_0)\,{\rm e}^{-\alpha|\sigma_i(t)|^p}\right)^2}\left[\varepsilon_i\hat{c}_{i_{\rm opt}}(t) - |d(t,x)|\right] . \end{aligned} \tag{28}$$

We have $\varepsilon_i \hat{c}_{i_{\rm opt}}(t) > |d(t,x)|$ and

$$\frac{K\left[\left(\sigma_0+(1-\sigma_0)\,\mathrm{e}^{-\alpha|\sigma_i(t)|^p}\right)+|\sigma_i(t)|(1-\sigma_0)\,\mathrm{e}^{-\alpha|\sigma_i(t)|^p}\alpha p|\sigma_i(t)|^{p-1}\right]}{\left(\sigma_0+(1-\sigma_0)\,\mathrm{e}^{-\alpha|\sigma_i(t)|^p}\right)^2}>0,$$

an upper boundary can be found as follows:

$$\begin{aligned}\dot{V}_i(t) \le & -\sqrt{2}\left\{\varepsilon_i\hat{c}_{i_{\rm opt}}(t)-|d(t,x)|\right\}\frac{|\sigma_i(t)|}{\sqrt{2}}\\ & -\frac{\sqrt{2}K\left[\left(\sigma_0+(1-\sigma_0)\,\mathrm{e}^{-\alpha|\sigma_i(t)|^p}\right)+|\sigma_i(t)|(1-\sigma_0)\,\mathrm{e}^{-\alpha|\sigma_i(t)|^p}\alpha p|\sigma_i(t)|^{p-1}\right]}{\left(\sigma_0+(1-\sigma_0)\,\mathrm{e}^{-\alpha|\sigma_i(t)|^p}\right)^2}\\ & \times\left[\varepsilon_i\hat{c}_{i_{\rm opt}}(t)-|d(t,x)|\right]\frac{\hat{c}_{i_{\rm opt}}(t)}{\sqrt{2}} \le -Z\left(\frac{|\sigma_i(t)|}{\sqrt{2}}+\frac{\varepsilon_i\hat{c}_{i_{\rm opt}}(t)}{\sqrt{2}}\right)\le -ZV_i(t)^{0,5},\end{aligned} \tag{29}$$

where Z is defined as follows:

$$Z=\sqrt{2}\left\{\varepsilon_i\hat{c}_{i_{\rm opt}}(t)-|d(t,x)|\right\}\min\left\{1,\frac{\sqrt{2}K\left[\left(\sigma_0+(1-\sigma_0)\,\mathrm{e}^{-\alpha|\sigma_i(t)|^p}\right)+|\sigma_i(t)|(1-\sigma_0)\,\mathrm{e}^{-\alpha|\sigma_i(t)|^p}\alpha p|\sigma_i(t)|^{p-1}\right]}{\left(\sigma_0+(1-\sigma_0)\,\mathrm{e}^{-\alpha|\sigma_i(t)|^p}\right)^2}\right\}.$$

Consequently, based on Eq. (29), according to Lemma 2 and Lyapunov's stability theorem, the suggested control law will achieve stability within a finite time.

5. Application of the suggested control on the chaotic PMSG

This section showcases numerical simulations that demonstrate and validate the effectiveness of the proposed method. The simulation outcomes are derived from a 300-kW PMSG wind turbine with the the initial states are considered as: $x(0)=[0.1,0.3,0.2]$. Initially, the normalized PMSG model outlined in Eq. (9) is broken down as follows:

$$\dot{x}=f(x)+d(t,x)+u(t), \tag{30}$$

$$f(x)=\begin{bmatrix}\varphi(x_2-x_1)+\varepsilon x_3x_2\\ -x_2-x_1x_3+\gamma x_1\\ -x_3+x_1x_2\end{bmatrix}, \tag{31}$$

where in Eq. (4), $x(t)=[x_1,x_2,x_3]^{\rm T}$ is the state vector of the system, $f(x)$ represents a specified vector field and illustrates the dynamic system represented in Eq. (31).

To achieve stabilization of the PMSG system at its equilibrium point $(0,0,0)^{\rm T}$, we define the control input $u(t)$ as follows:

$$u(t)=[u_1,u_2,u_3]^{\rm T}=\left[\tilde{T},\tilde{u}_{\rm q},\tilde{u}_{\rm d}\right]^{\rm T}. \tag{32}$$

Remark 4 It is well established that time does not play a role in dynamics. Since Liu's chaotic system is time-independent, the function $f(t,x)$ has been utilized in Eqs. (30) and (31) in place of $f(x)$.

Remark 5 To ensure a fair comparison of the three controllers in this study, the initial state values were set to $x(0)=[0.1,\,0.3,\,0.2]^{\rm T}$. It is important to clarify that the initial values of a chaotic PMSG system are unique and determine its chaotic behavior. Modifying these initial conditions can potentially prevent the system from entering a chaotic state.

After executing the required calculations using Theorem 1, we obtain the chatter-free TSMC based on the adaptive exponential reaching barrier function law for the above-defined system as follows:

$$\begin{aligned}\dot{u}_1 &= -(\lambda_1+k_1)(u_1+\varphi(x_2-x_1)+\varepsilon x_3x_2)-[-\varphi\dot{x}_1+(\varphi+\varepsilon x_3)\dot{x}_2+\varepsilon x_2\dot{x}_3]-\lambda_1k_1x_1-\varepsilon_1\hat{c}_{1_{\rm opt}}\,\mathrm{sign}(\sigma_1),\\ \dot{u}_2 &= -(\lambda_2+k_2)(u_2-x_2-x_1x_3+\gamma x_1)-[(\gamma-x_3)\dot{x}_1-\dot{x}_2-x_1\dot{x}_3]-\lambda_2k_2x_2-\varepsilon_2\hat{c}_{2_{\rm opt}}\,\mathrm{sign}(\sigma_2),\\ \dot{u}_3 &= -(\lambda_3+k_3)(u_3-x_3+x_1x_2)-[x_2\dot{x}_1+x_1\dot{x}_2-\dot{x}_3]-\lambda_3k_3x_3-\varepsilon_3\hat{c}_{3_{\rm opt}}\,\mathrm{sign}(\sigma_3),\\ \dot{\hat{c}}_{1_{\rm opt}}(t) &= \frac{K|\sigma_1(t)|}{\sigma_0+(1-\sigma_0)\,\mathrm{e}^{-\alpha|\sigma_1(t)|^p}},\\ \dot{\hat{c}}_{2_{\rm opt}}(t) &= \frac{K|\sigma_2(t)|}{\sigma_0+(1-\sigma_0)\,\mathrm{e}^{-\alpha|\sigma_2(t)|^p}},\\ \dot{\hat{c}}_{3_{\rm opt}}(t) &= \frac{K|\sigma_3(t)|}{\sigma_0+(1-\sigma_0)\,\mathrm{e}^{-\alpha|\sigma_3(t)|^p}}.\end{aligned} \tag{33}$$

In order to accurately evaluate the simulation results of the suggested method, the controller parameters are meticulously set to identical values across all three approaches. This uniformity is essential for making a fair comparison with the outcomes detailed in Refs. [22,47]. By maintaining consistent parameters, we can ensure that any differences observed in performance can be attributed solely to the variations in the methods being tested. This systematic approach will enhance the reliability of our findings and contribute to the overall validity of the evaluations conducted.

The parameters of the control law align precisely with those outlined in Ref. [22]. They are chosen as: $\varepsilon_1 = 5$, $\varepsilon_2 = 4$, $\varepsilon_3 = 4$, $\lambda_i = 1$, $k_i = 1$, $i = 1, \ldots, 3$, and the parameter of the initial values are taken into account as: $x(0) = [0.1, 0.3, 0.2]^{\mathrm{T}}$. The exponential reaching law parameters: $\delta_0 = 0.08$, $\alpha = 1000$, $p = 2$, and $K = 3$. To conduct the simulation, we will input the values of the previously mentioned control parameters into Eq. (33).

Figures (5a), (5b), and (5c) illustrate the angular speed ω, quadrature current i_{q}, and direct current i_{d}, respectively, as they controlled at $t = 10$ s. To demonstrate the effectiveness of the method proposed in this paper, we compare our results with those obtained in Refs. [22,47]. Table 1 presents numerical data detailing the overshoot and undershoots for each state variable across the three methods.

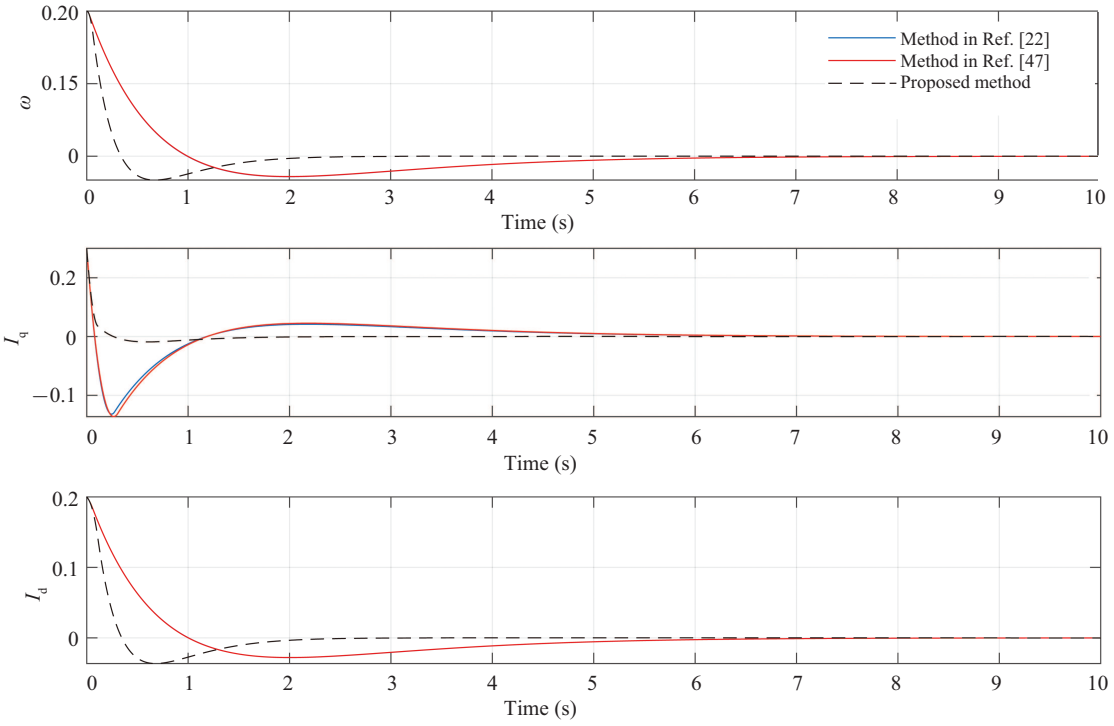


Fig. 5. Comparisons of state variables in chaotic PMSG trajectories using the proposed approach with the methods in Refs. [22,47].

Table 1. Quantitative comparisons of transient system specifications of the control methods.

PMSG	Method in Ref. [22]			Method in Ref. [47]			Proposed method		
State variables	w	i_{q}	i_{d}	w	i_{q}	i_{d}	w	i_{q}	i_{d}
Overshoot		0.04186	0	0	0.04529	0	0	0	0
Undershoot	0.01410	−0.2639	−0.02798	−0.01402	−0.2723	−0.02791	−0.01396	−0.00560	−0.02781

Compared to those controllers in Refs. [22,47], the suggested controller provides superior performance with no overshoot and improved undershoot values, making it a more stable and reliable method compared to the others. The methods proposed in Refs. [22,47] show higher overshoot and undershoot values, particularly for i_{q}, indicating less stability in this aspect. Figure 6 illustrates the influence of the control parameter selections on the simulation results. It is evident that the appropriate tuning of the parameters within the adaptive exponential reaching law significantly affects the system's performance. This highlights the critical importance of the parameter selections in achieving accurate and stable control outcomes.

Based on the results presented, it is evident that the proposed method outlined in this paper significantly outperforms existing approaches in terms of effectiveness, stability, and ini-

tial consistency. These attributes are particularly important in applications where immediate and reliable performance is not just beneficial, but essential for success. Therefore, the advantages offered by this method could make a substantial difference in real-world scenarios where users depend on fast and dependable outcomes. Ultimately, this reinforces the relevance of the proposed method for practical applications requiring high standards of performance.

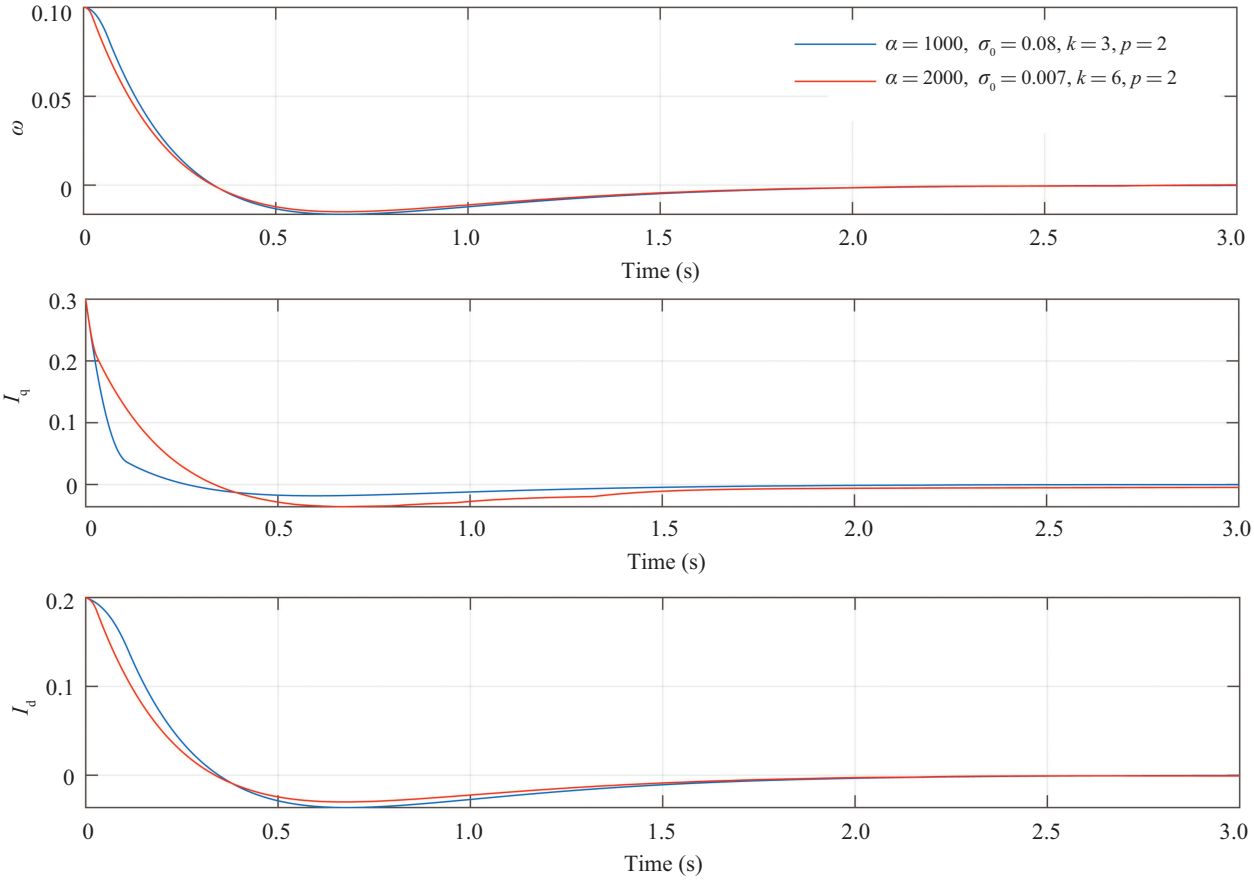


Fig. 6. The effect of the adaptive exponential reaching law parameters on the simulation results.

6. Conclusion

This paper provides an in-depth analysis of controlling a chaotic PMSG wind turbine by employing chatter-free and finite-time sliding mode control strategies, which are fundamentally based on adaptive exponential reaching control as well as Lyapunov's stability theory. The innovative control scheme introduced in the study utilizes a smooth and continuous control law, effectively addressing and eliminating the significant chattering problem typically associated with conventional sliding mode controllers that depend on a discontinuous sign function. Comprehensive results highlighted in the research demonstrate that the proposed control method not only successfully eradicates chattering but also sustains strong and robust performance in chaotic systems, even in the presence of unknown uncertainties and external disturbances. Overall, the findings underscore the potential of this advanced control approach for enhancing the stability and reliability of PMSG wind turbines operating under chaotic conditions.

Appendix: Some parameters

(i) Parameters of the PMSG

$R_s = 4578\ \Omega$, $L_d = 334$ mH, $L_q = 358$ mH, $P = 2$, $\emptyset_f = 3$ Wb, $f = 0003035\ \mathrm{Nm \cdot m \cdot rad^{-1} \cdot s^{-1}}$, $T = 8\ \mathrm{N \cdot ms}$.

(ii) Characteristics of simulated WT

Blades = 3, $R = 14$ m, $J = 50\ \mathrm{kg \cdot m^2}$, $P_w = 300$ kW, $\rho = 122$, $G = 23$.

(iii) Control law parameters

$\alpha = 1000$, $K = 3$, $p = 2$, $\sigma_0 = 0.08$.

References

[1] Tong W 2010 *Wind Power Generation and Wind Turbine Design* (WIT Press)
[2] Ashuri T, Zaaijer M B, Martins J R, Van Bussel G J and Van Kuik G A 2014 *Renew. Energy* **68** 893
[3] Burton T, Jenkins N, Sharpe D and Bossanyi E 2011 *Wind Energy Handbook* (John Wiley & Sons)
[4] Mechter A, Kemih K and Ghanes M 2016 *Nonlinear Dyn.* **84** 2435
[5] Rolan A, Luna A, Vazquez G, Aguilar D and Azevedo G 2009 *Proc. IEEE Int. Symp. Ind. Electron.* 734
[6] Luo N, Vidal Y and Acho L (ed.) 2014 *Wind Turbine Control and Monitoring* (Springer Int. Publ., Basel)

[7] Li Z, Park J B, Joo Y H, Zhang B and Chen G 2002 *IEEE Trans. Circuits Syst. I* **49** 383
[8] Zheng X, Li H, Song R and Feng Y 2016 *Proc. IEEE Conf. Ind. Electron. Appl.* 2419
[9] Yu J, Yu H, Chen B, Gao J and Qin Y 2012 *Nonlinear Dyn.* **70** 1879
[10] Maeng G and Choi H H 2013 *Nonlinear Dyn.* **74** 571
[11] Choi H H and Jung J W 2012 *Nonlinear Dyn.* **67** 1717
[12] Choi H H 2012 *Nonlinear Dyn.* **69** 1311
[13] Karimi A, Akbari H, Mousavi S and Beheshtipour Z 2023 *Syst. Sci. Control Eng.* **11** 2207593
[14] Boccaletti S, Grebogi C, Lai Y C, *et al.* 2000 *Phys. Rep.* **329** 103
[15] Chen Y and Leung A Y T 2012 *Bifurcation and Chaos in Engineering* (Springer)
[16] Rajagopal K, Karthikeyan A and Duraisamy P 2017 *Nonlinear Eng.* **6** 79
[17] Ott E, Grebogi C and James A 1990 *Phys. Rev. Lett.* **64** 1196
[18] Li H, Liao X, Li C and Li C 2011 *Neurocomputing* **74** 3212
[19] Takhi H, Kemih K, Moysis L, *et al.* 2021 *Math. Comput. Simul.* **181** 150
[20] Wang S, Yousefpour A, Yusuf A, Jahanshahi H, Alcaraz R, He S and Munoz-Pacheco J M 2020 *Entropy* **22** 271
[21] Ablay G 2009 *Nonlinear Anal.: Hybrid Syst.* **3** 531
[22] Zhang X, Liu X and Zhu Q 2014 *Appl. Math. Comput.* **232** 431
[23] Lin W 2008 *Phys. Lett. A* **372** 3195
[24] Roldán-Caballero A, Pérez-Cruz J H, Hernández-Márquez E *et al.* 2023 *Complexity* **2023** 2881192
[25] Zhang H, Qin H and Chen G 1998 *Int. J. Bifurcat. Chaos* **8** 2041
[26] Johansyah M D, Sambas A, Vaidyanathan S *et al.* 2024 *Nonlinear Dyn. Syst. Theory* **24** 275
[27] Kemih K, Halimi M, Ghanes M, *et al.* 2014 *Eur. Phys. J. Spec. Top.* **223** 1579
[28] Takhi H, Kemih K, Moysis L *et al.* 2020 *Int. J. Dyn. Control* **8** 973
[29] Kemih K 2009 *Chaos Solitons Fractals* **41** 1897
[30] Takhi H, Kemih K, Moysis L, Volos C, Kemih K and Ghanes M 2020 *Int. J. Dyn. Control* **8** 973
[31] Messadi M, Mellit A, Kemih K, *et al.* 2014 *Nonlinear Phenom. Complex Syst.* **17** 183
[32] Takhi H, Moysis L, Machkour N, *et al.* 2022 *Eur. Phys. J. Spec. Top.* **231** 443
[33] Chen J and Shi Y 2021 *Philos. Trans. R. Soc. A* **379** 20200371
[34] Messadi M, Mellit A, Kemih K and Ghanes M 2015 *Chin. Phys. B* **24** 010502
[35] Hamiche H, Kemih K, Ghanes M, *et al.* 2011 *Nonlinear Anal.* **74** 1146
[36] Kemih K, Kemiha A and Ghanes M 2009 *Chaos Solitons Fractals* **42** 735
[37] Kemih K, Bouraoui H, Messadi M, *et al.* 2013 *Acta Phys. Pol. A* **123** 193
[38] Shao K, Zheng J, Tang R, Li X, Man Z and Liang B 2022 *IEEE/ASME Trans. Mechatronics* **27** 4258
[39] Laghrouche S, Harmouche M, Chitour Y, Obeid H and Fridman L M 2021 *Automatica* **123** 109355
[40] Mobayen S, Alattas K A and Assawinchaichote W 2021 *IEEE Trans. Circuits Syst. I* **68** 4403
[41] Xiu C and Guo P 2018 *IEEE Access* **6** 49793
[42] Drakunov S V and Utkin V I 1992 *Int. J. Control* **55** 1029
[43] Plestan F, Shtessel Y, Bregeault V and Poznyak A 2010 *Int. J. Control* **83** 1907
[44] Dong Z and Ma J 2020 *IEEE Access* **8** 143359
[45] Sepestanaki M A, Bahmani H, Ali M A, Jalilvand A, Mobayen S and Fekih A 2022 *IEEE Access* **10** 34296
[46] Obeid H, Fridman L M, Laghrouche S and Harmouche M 2018 *Automatica* **93** 540
[47] Sepestanaki M A, Barhaghtalab M H, Mobayen S, Jalilvand A, Fekih A and Skruch P 2022 *IEEE Access* **10** 103469
[48] Mechter A, Kemih K and Ghanes M 2015 *Acta Phys. Pol. Hung.* **12** 167